Article

Evaluation of the Applicability of Voltammetric Modes in Scanning Electrochemical Microscopy for In Situ Corrosion Characterisation of Copper-Based Materials

Brenda Hernández-Concepción [1], Adrián Méndez-Guerra [1], Ricardo M. Souto [1,2,*] and Javier Izquierdo [1,2,*]

1   Department of Chemistry, Universidad de La Laguna, P.O. Box 456, Tenerife, 38200 La Laguna, Spain; hernandez.concepcion.39@ull.edu.es (B.H.-C.); alu0101121246@ull.edu.es (A.M.-G.)
2   Institute of Material Science and Nanotechnology, Universidad de La Laguna, P.O. Box 456, Tenerife, 38200 La Laguna, Spain
*   Correspondence: rsouto@ull.es (R.M.S.); jizquier@ull.edu.es (J.I.)

Abstract: Chemical imaging of corrosion processes involving copper species using scanning electrochemical microscopy has been hampered by the lack of soluble oxidation states for copper that can be achieved by amperometric conversion at the tip. Indeed, the only possibility is to reduce the corrosion products at the tip, thus modifying the chemical response of the electrode material and requiring subsequent redissolution of the copper deposits. Consequently, the limitations arising from the system prevented a full-scale quantification, requiring the development of new methodologies or the optimisation of those currently available, as we pursued with the present work. Therefore, the voltammetric behaviours of gold macro- and microelectrodes were evaluated with respect to the collection and redissolution of Cu^{2+} ions, with the aim of using them as sensing probes in scanning electrochemical microscopy (SECM) to investigate the activity of copper surfaces in acidic chloride-containing environments. Cyclic and square-wave voltammetric techniques were explored for copper collection and subsequent stripping on Au microelectrode tips in SECM with the objective to capture in situ image electrochemical reactivity distributions across copper surfaces undergoing corrosion.

Keywords: square-wave voltammetry; cyclic voltammetry; gold microelectrode; anodic stripping; copper corrosion; scanning electrochemical microscopy

1. Introduction

The performance of metallic components is often limited by the loss of their properties due to environmentally induced degradation. Advanced research in corrosion science mainly aims for a better understanding of the surface chemical processes involved in the micrometre and submicrometre range, thus promoting the efficient and durable application of metallic materials to new societal expectations. To better control corrosion and its effects, researchers must integrate emerging advances in many areas of science and technology to understand mechanistic effects and relate them to underlying structures, compositions, and dynamics.

It has long been known that corrosion processes start at micrometre or nanometre scales [1], although until recently no suitable techniques were available to study reactions at such scales. Additionally, surface chemical heterogeneity is frequently observed for many metallic materials, particularly when dealing with alloys or joined (i.e., galvanically coupled) metals [2,3], but this can also occur with individual metallic materials that were once mistakenly considered stable and uniform in their passive state, examples of which are stainless steels [1,4] and prosthetic-quality titanium [5]. The issue of surface inhomogeneity is even more relevant when corrosion protection methods involve the chemical modification of surfaces [6]. Progress in corrosion research will therefore depend on the availability of experimental techniques capable of probing materials with higher spatial resolution and

shorter time scales that can provide new or additional evidence of reaction mechanisms, preferably in situ, or even in operation. In this context, the use of scanning electrochemical microscopy (SECM) in corrosion science has been shown to be a powerful technique [7,8].

SECM uses microelectrodes as probes to detect electrochemical reactivity at metal/elect rolyte interfaces [9–11]. By scanning the tip of a moving microelectrode (integrated active microdiscs with a typical diameter between 10 and 25 µm) near a surface immersed in an electrolyte solution, an image is obtained revealing local information about the chemical reactions and surface properties that take place in the volume of the solution between the tip and the sample. However, the application of SECM to the study of corrosion reactions has been significantly slower than that for other electrochemical applications [12–15], partly because in its early stages SECM was mainly an amperometric and potentiostatic technique. Although attractive advantages were recognised in regard to performing local quantitative electrochemical experiments, the possibility of using all the electrochemical techniques on both the probe and the substrate, and the possibility of coupling in situ electrochemical measurements with other techniques [16], their application to corrosion systems was limited by the requirement of a redox process at the tip for imaging (i.e., feedback mode). In fact, the addition of a redox mediator to the solution for its faradaic conversion at the tip would inevitably generate a Nernst potential at the metal surface under investigation, which may significantly alter the spontaneous mixed potential state of the corrosive system [11], and thus produce changes in the mechanism of the process under investigation. Advances have resulted from the adaptation of other operating modes, such as the generation-collection mode, usually in a configuration where the sample generates the chemical species that is collected and monitored at the tip (Substrate Generation-Tip Collection, SG-TC), and a modified Redox Competition mode (RC-SECM), which are illustrated schematically in Figure 1. As an illustration, two features of different chemical reactivity have been drawn on a flat insulating surface. The flat insulating surface produces no detectable signal at the microelectrode tip for SG-TC, potentiometric and RC-SECM modes (i.e., the green colour corresponds to a zero signal), while in feedback mode the tip picks up a signal that is smaller than in the bulk of the solution (i.e., the blue colour represents a negative feedback response). The first feature is an insulating bump (coloured brown on the topographic map) that is not visulaised in SG-TC, RC-SECM and potentiometric modes (thus coloured green), but is detected using feedback mode as a greater negative feedback (darker blue). The second feature is a hole in the surface due to a chemically active site corroding in the electrolyte. In this case, soluble corrosion products are detected as anodic (positive) currents at the tip in SG-TC mode, and as a positive concentration signal in potentiometric mode (coloured red/yellow). This hole is also detected with the amperometric tip in RC-SECM mode, although this time it involves soluble species from the cathodic half-cell reaction (as a blue-coloured negative current). Since the site is chemically active, regeneration of the redox mediator used in the feedback mode leads to a higher (more positive) current, which is shown in red. The illustrated amperometric modes require the redox conversion of some species to another oxidation state, whereas potentiometric modes are selective to a certain oxidation state without redox conversion. In feedback mode, the current increases over the active domains capable of regenerating a redox mediator added to the electrolyte phase, and also responds to the morphology of electrochemically inactive surfaces due to the hindered diffusion of the redox mediator towards the probe.

As result, SECM has gained increasing interest and application, especially over the past fifteen years, with significant achievements in the study of pitting initiation and propagation [17,18], galvanic pair formation [19–21], the resolution of surface microstructures [22–24], stress corrosion [25,26], and the investigation of electron transfer kinetics in passive oxide layers [27,28]. In addition, it is also used to establish the effectiveness of different corrosion protection schemes or technologies, including coatings [29–31] or surface treatments [32–34]. On the other hand, ion-selective microelectrodes have also been employed as SECM tips in a potentiometric operation [35].
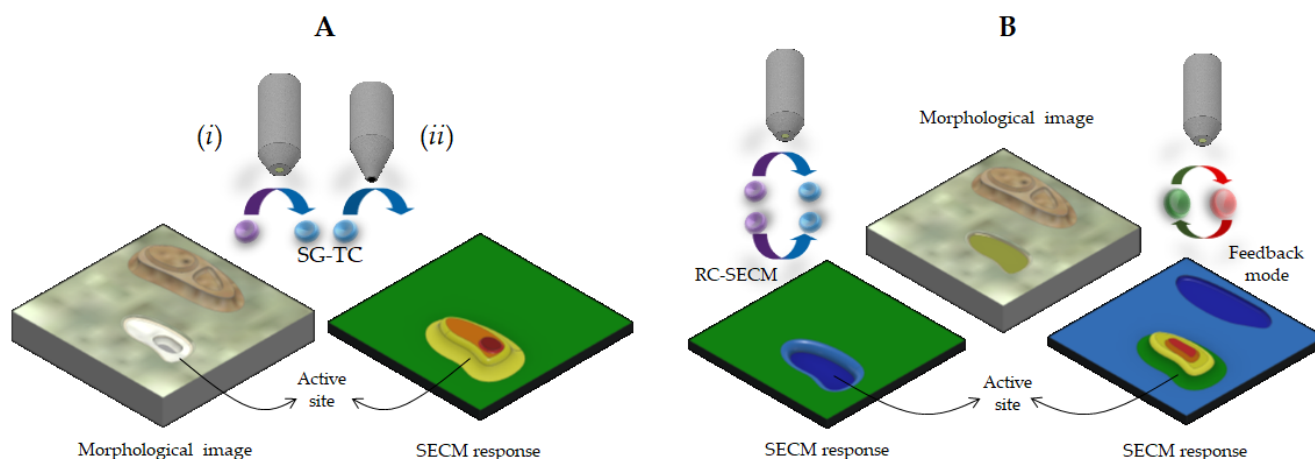
Figure 1. Schematic of the various operation modes in SECM, where yellow-red colours correspond to positive signals (i.e., current or potential) and blue colour reflects signals below those registered over inactive areas (green coloured). (**A**) Substrate generation-tip collection (SG-TC) mode responding to concentration gradients of target species on active sites through (*i*) its electrochemical conversion at an amperometric tip or (*ii*) selective potentiometric detection using an ion-selective tip. (**B**) Amperometric redox-competition (RC-SECM) and feedback responses on a surface exhibiting active domains and topographic features. RC-SECM exhibits current decrease (more negative) over the active domains competing for the same sensed species.

Unfortunately, the corrosion of copper-based materials using SECM has been greatly limited by the deposition of copper metal on the tip, since there is no other oxidation state available for redox conversion that would be soluble in the electrolyte. In this way, despite some promising results on copper dissolution in acidic environments using a combined AFM–SECM operation, chemical information could not be resolved with spatial resolution since the metal was collected during a complete line scan and could only be quantified from the charge measured at the tip during its stripping. In this way, all the copper was re-dissolved independently of the actual location on the surface where it was collected. Only Cu-ISME electrodes could be thus employed to overcome that limitation to the generation-collection mode [36]. Alternately, studies on the corrosion inhibition of copper-based materials were almost exclusively based on the feedback mode of operation [37], despite the unavoidable modification of the electrical condition of the metal surface due to the Nernst potential resulting from the redox couple necessary in this mode.

An attractive procedure to overcome these limitations would be the application of voltammetric routines to the SECM tip, which would allow one to combine copper collection and stripping steps with the rastering movement of the tip in SECM imaging. This experimental approach was already used to investigate copper corrosion in an acidic environment by building an SECM tip around an AFM cantilever, thus leading to the simultaneous imaging of the corroding surface using the AFM operation, whereas a signal related to copper dissolution was obtained with the built-in SECM tip [38]. Unfortunately, copper dissolution could not be directly associated with specific locations in the corroding surface because it was deposited in the tip along the scan, and its subsequent stripping corresponded to the total deposited copper. Furthermore, quantification was also difficult because the shape of stripping voltammogram changed with the potential applied to the corroding substrate, that is, effectively changing with varying corrosion rates [39]. But spatial resolution has been described in the literature in the case of a hyphenated technique named fast-scan cyclic voltammetry-scanning electrochemical microscopy [40,41], which has been successfully employed to study the biological activity of single cells, as well as for the identification of metal cations in electroanalytical experiments, although through the use of tips modified with mercury [41]. In the latter case, a hemispherically-shaped droplet

was deposited on the surface of the microelectrode tip, which affected the spatial resolution of the method.

It is established in the literature that gold is the best-suited electrode material for the collection and stripping of copper, and it has been selected in our work accordingly. Although there are studies available on this subject using both macroelectrodes and microelectrodes, the range of concentration of the dissolved copper ions usually investigated in the latter case are typical of electroanalytical applications, which are significantly smaller than those usually found locally in corrosion studies. Therefore, in this work we have investigated the electrochemical characteristics of Au electrodes of disc shapes of varying diameter sizes corresponding to macro- and microelectrode dimensions for the collection and the stripping of copper in a 3.5 wt.% NaCl solution (a test environment frequently employed in corrosion studies due to presenting a similar ionic strength and chloride content to seawater). Finally, preliminary experiments on the applicability of SECM combined with voltammetric modes for the imaging of a corroding surface of copper in 3.5 wt.% NaCl solution are also reported. It is envisaged that the methodology developed in this work can be employed to investigate localised corrosion processes of copper-containing metallic materials.

2. Materials and Methods

2.1. Materials

Gold (Au) electrodes were built by encasing metal wires in glass capillaries by means of a micropipette puller. In this way, glass-embedded discs were exposed at the end of the elongated pipette tip, while electrical contact between the Au wire and a Cu connector was ensured in the lumen of the pipette assembly using a conductive Au-epoxy glue. Au wires of 150 and 10 µm diameters were employed to reproduce the electrochemical behaviours of macro- and microelectrodes, respectively. The surface of the Au electrodes was finished using 4000-grit silicon carbide paper followed by polishing using 1 µm alumina suspension.

Corrosion testing was firstly performed on a copper sample fabricated by cutting a 2.7×2.0 cm^2 area from a 99.99% purity plate of 1 mm thickness purchased from Goodfellow (Cambridge, UK), and mounted in Epofix$^®$ epoxy resin (Struers, Copenhagen, Denmark). A second sample was fabricated using the same procedure from a copper wire of 125 µm diameter to minimise border effects. Before electrochemical testing, the surface of the samples was abraded using a sequence of emery papers up to 4000 grit, followed by polishing with 1 µm alumina particles in water suspension. The samples were cleaned in an ultrasonic bath with water and dried in warm air.

Analytical grade reagents were used to prepare the solutions employed in this work by dissolving them in Milli-Q grade purified water (Millipore, Burlington, MA, USA). Ferrocene-methanol (Aldrich, St. Louis, MO, USA) was added to the test solutions as a redox mediator for SECM operation in feedback mode.

2.2. Methods

The electrochemical measurements were carried out using a Sensolytics electrochemical workstation for scanning electrochemical microscopy (SECM), which was built around an Autolab bipotentiostat/galvanostat (Metrohm, Herisau, Switzerland). The small microelectrochemical cell and the motors for SECM operation were placed on a vibration isolation table and all housed inside a Faraday cage for the stable measurement of currents in the order of nA. Conventional voltammetric operation was performed in the bulk of the electrochemical cell in a three-electrode configuration, with the Au electrode as the primary working electrode, and an Ag/AgCl/KCl (sat.) and a Pt grid as reference and auxiliary electrodes, respectively. The second working electrode connection was not employed in the conventional voltammetric measurements. Tests were performed in 3.5 wt.% NaCl solution, acidified to pH 3.5 by adding minute volumes of a concentrated HCl solution. The voltammetric techniques chosen were cyclic and square-wave voltammetries. When the copper sample was tested for corrosion characterisation, this was connected to the

workstation using the secondary working electrode connection, allowing the sample to be imaged under potentiostatic polarisation when desired. The Au microelectrode of 10 μm diameter remained connected to the primary working electrode connection, and its positioning in the cell was controlled using the *XYZ* motors of the SECM assembly. Accurate positioning relative to the sample was achieved using the SECM feedback mode [11] by recording *Z*-approach curves using ferrocene-methanol added to the test solution in 0.5 mM concentration as redox mediator. Scans were performed in an *XY* plane parallel to the surface of the copper sample with a tip-sample distance of 10 μm using a scanning rate of 30 μm s^{-1}.

3. Results and Discussion

3.1. Electrochemical Behaviour of Gold Electrodes for Copper Collection and Redissolution

The behaviour of a gold disc electrode of 500 μm diameter was first evaluated in regard to its ability to collect and re-dissolve Cu^{2+} in the bulk of an aqueous solution. Figure 2 shows the cyclic voltammogram recorded in a 3.5 wt.% NaCl stock solution, and with the addition of 100 mM $CuCl_2$. The potential, *E*, was first swept in the anodic direction from −0.50 up to +0.40 V, and then reversed to the initial potential.
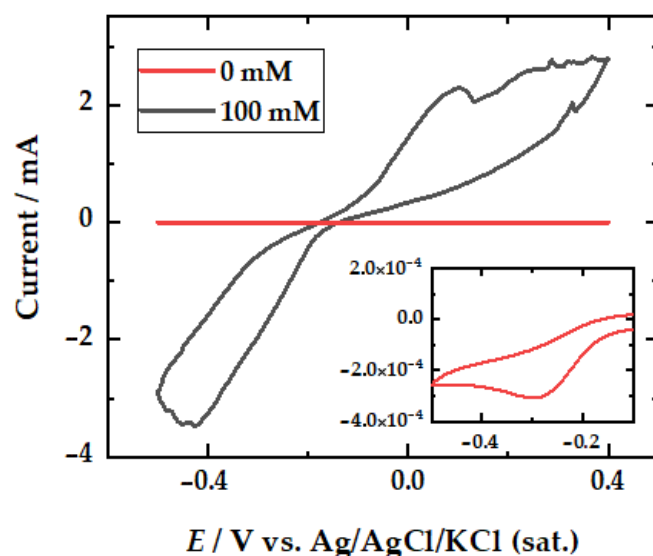

Figure 2. Cyclic voltammograms recorded for a gold electrode of 500 μm diameter in 3.5 wt.% NaCl + *x* mM $CuCl_2$ solutions adjusted to pH 3.5 (with *x* = 0, 100 as indicated in the figure). Scan rate: 0.05 V s^{-1}. The inset shows an enlargement of the plot obtained for the solution not containing $CuCl_2$.

The voltammogram recorded in the 3.5 wt.% NaCl solution is characterised by showing only the signal corresponding to the electroreduction of dissolved oxygen in the electrolyte, appreciable between −0.3 and −0.4 V (see the inset of the figure). The half-reaction in Equation (1) takes place when a sufficient cathodic potential is applied, in naturally aerated solutions. However, this contribution to the total current (*I*) may become almost negligible in the presence of other electroactive species, such as Cu^{2+} ions, depending on the concentration of those species. Thus, the voltammogram performed in the presence of Cu^{2+} cations at a concentration of 100 mM for the macroelectrode corresponds to the situation described above, since the redox processes corresponding to their reduction on the gold electrode and their subsequent reoxidation originate current values ca. 10^4 times greater than the current values measured for the oxygen reduction in Figure 2. It must be noted that the shape of the voltammogram differs notably from that of a typical reversible redox system, which shows symmetrical oxidation and reduction waves when there is no kinetic hindrance. In addition, it is recorded that the potential difference between the anodic and cathodic peaks amounts to almost 500 mV. Therefore, although reversibility of

the Cu^{2+}/Cu redox process could be expected on the basis of thermodynamic data, kinetic factors must operate at the working electrode that effectively influence this reaction [42].

$$O_2 + 2\,H_2O + 4e^- \rightarrow 4\,OH^- \qquad (1)$$

Although the experimental conditions were the same, the microelectrode response in Figure 3 shows major differences with respect to the behaviour of the macroelectrode given in Figure 2, thus preventing the use of published data on copper deposition on conventional Au electrodes for the choice of operation parameters for that process in scanning electrochemical microscopy. Therefore, prior characterisation of the deposition and stripping parameters based on voltammetric techniques must be performed using a tip microelectrode of the same dimensions as those to be employed as the SECM-tip. Firstly, the order of magnitude of the current is lower, not exceeding the range of μA since, the active surface of the electrode being smaller, the amount of copper that can be deposited and re-dissolved will be also lower. Secondly, no O_2 reduction peak is observed on the voltammogram carried out in the 3.5 wt.% NaCl solution (see Figure 3A), but only the onset of a reduction current which does not reach a stationary value in this potential range. It must be taken into account that such a reversible two-electron redox process at a microelectrode does not cause a current peak in a voltammogram, but instead gives rise to a diffusion-dependent platform of the electroactive species if the scan rate is not too high. However, deviations from this ideal behaviour are observed when the electroactive species to be transformed exhibits higher mobility, requiring longer time (slower scan rate) and/or higher overpotential to reach a diffusion-controlled value. Therefore, these features observed in Figure 3 can be justified comparing the diffusion coefficients of oxygen (2.20×10^{-5} cm^2 s^{-2}) with respect to a better-defined diffusion current species such as ferrocene-methanol ($D = 7.60 \times 10^{-6}$ cm^2 s^{-2}) [43,44].
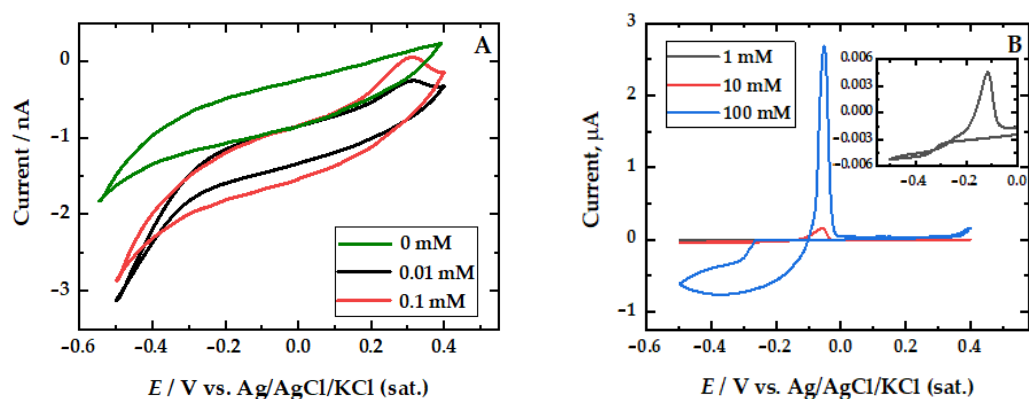

Figure 3. Cyclic voltammograms recorded for a gold microelectrode of 10 μm diameter in 3.5 wt.% NaCl + x mM CuCl$_2$ solutions adjusted to pH 3.5. (**A**) For $0 \le x \le 0.1$ and (**B**) for $1 \le x \le 100$ as indicated in the plots. Scan rate: 0.05 V s^{-1}.

On the other hand, the cyclic voltammogram measured at the microelectrode in the solution containing 100 mM CuCl$_2$ in Figure 3B provides different information from that provided by the macroelectrode under the same conditions, consistent with other reports conducting deposition and dissolution of copper in gold microelectrodes [45]. When the applied potential is sufficiently cathodic to cause the reduction of the Cu^{2+} cations on the gold microdisc without kinetic interference, a current peak is defined as the current becomes controlled by mass transfer (diffusion). Since the gold surface has become completely covered by metallic copper, the subsequent reduction of copper ions is deposited on metallic copper instead of gold, leading to a greater electrode area that is observed as a small current increase at a potential close to the anodic switch potential. Copper dissolution occurs during the cathodic sweep at potentials below 0 V. From the foregoing, not only does it seem convenient to use microelectrodes to detect the amount of Cu^{2+} ions present on a surface generating a local response, but even at relatively high

concentrations such as 0.1 M, the detected signals are better defined and more quantifiable in the case of microelectrodes due to the dependence of the current on diffusion processes.

The behaviour of the microelectrode as a function of Cu^{2+} concentration can be deduced from the observation of the cyclic voltammograms in Figure 3. The voltammograms in Figure 3B follow the same events already discussed for the 100 mM Cu^{2+} concentration. The cathodic current due to the reduction of copper below -0.3 V increases proportionally to the concentration of Cu^{2+}, although the onset of copper reduction in a 0.1 mM solution is only clearly revealed at more cathodic potentials. The voltammogram in the 0.01 mM solution did not provide clear signals, rendering it ineffective for copper determination using this procedure at such low concentration ranges (see Figure 3A). A second minor peak, presumably revealing Cu(I) to Cu(II) conversion, seems to emerge around 0.25 V, yet major oxidation of nearly all deposited Cu^0 to Cu(I) species occurs in the first peak, as expected in a highly concentrated chloride solution [46]. An oxygen reduction reaction is likely to occur and the electrocatalytic behaviour of the probe towards this reaction will certainly change when copper is deposited, both regarding over-potential and current density. Based on these observations, a semiquantitative correlation between the voltammetric response at the Au microelectrode and the Cu^{2+} concentration can be attempted by choosing a characteristic parameter from the voltammograms, either the integration of the voltammetric peak around -0.1 V or the limiting cathodic current measured at -0.3 V, as they are shown in Figure 4.
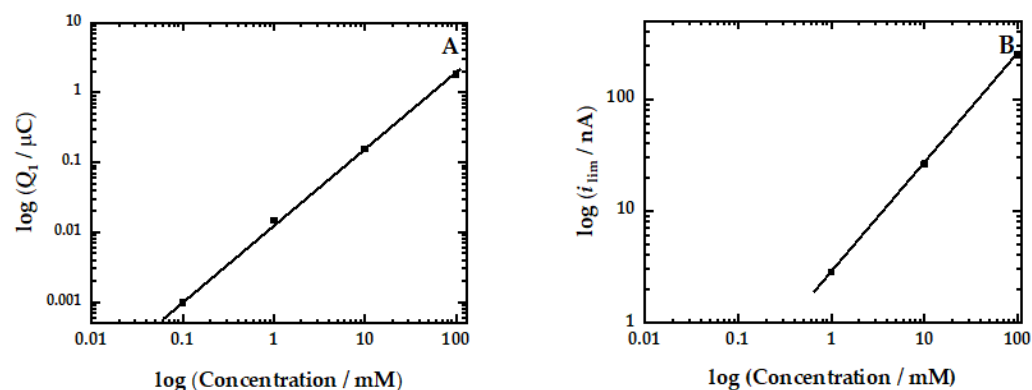

Figure 4. Dependence with the concentration of Cu^{2+} ions for selected signals observed in the voltammetric data of Figure 3. (**A**) Integration of the voltammetric peak occurring in the cyclic voltammograms around -0.1 V and (**B**) limiting cathodic current measured at -0.3 V.

Concerning the square-wave voltammograms in Figure 5, it should be noted that the main signal differs according to the Cu^{2+} in the solution to be electrodeposited. Whereas the low concentration range results in anodic stripping at around $+0.35$ V (cf. Figure 5A), all the voltammograms obtained at CuCl concentrations 1 mM or higher exhibit a signal which is only clearly identifiable in a lower range of potentials. That is, the voltammogram provided a bulk copper reoxidation signal at the $-0.2 < E < 0$ V potential range as seen in Figure 5, except for those measurements registered at 0.01 and 0.1 mM in Cu^{2+}, which only resulted in one much smaller copper oxidation peak at around $+0.35$ V. The latter reoxidation potential is known to be due to the copper underpotential deposition (UPD) phenomena, which renders a Cu deposit directly attached to gold, and may lead to saturation of the gold surface. Reoxidation at less anodic conditions (namely $-0.2 < E < 0$ V) stems from the breakdown of bulk copper (Cu–Cu interactions) which requires lower energy for redissolution. In this case, quantification of the Cu ion concentration based on the square-wave voltammetric data can also be carried out as shown in Figure 6, although a different parameter must be selected depending on whether low or high Cu^{2+} ion concentrations are involved.
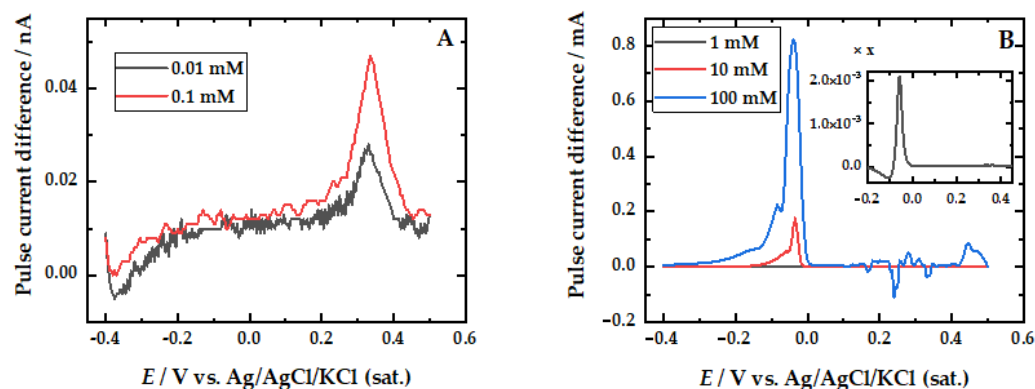
Figure 5. Square-wave voltammograms recorded for a gold microelectrode of 10 μm diameter in 3.5 wt.% NaCl (pH 3.5) + *x* mM CuCl$_2$ solution. (**A**) For $x \leq 0.1$ and (**B**) for $1 \leq x \leq 100$, as indicated in the plots. Deposition time: 10 s.
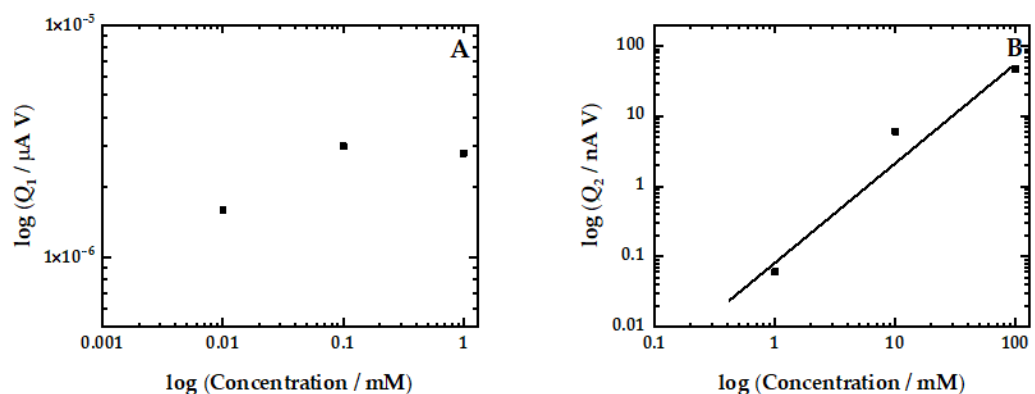

Figure 6. Dependence with the concentration of Cu^{2+} ions for some relevant signals observed in the square-wave voltammograms of Figure 5. The plots show the integration of the square-wave voltammetric peaks recorded around (**A**) +0.35 and (**B**) −0.1 V, respectively.

Interestingly, the voltammetric signal recorded in the 1 mM solution showed not only a reoxidation peak at −0.06 V, ascribed to Cu-Cu cleavage (see inset in Figure 5B), but a copper reoxidation stripping signal can also be distinguished and quantified at approximately +0.35 V, very similar to that obtained for a concentration of copper 10 times lower. This tendency suggests that complete coverage of the gold surface at sufficient copper deposition (i.e., sufficient copper concentration) derives to gold saturation due to the underpotential deposition of copper, and the most anodic reoxidation peak cannot be used as a quantifiable signal. The peak at +0.35 V is not distinguishable from the voltammetric measurements conducted at 10 and 100 mM (cf. Figure 5B), but this does not imply that the underpotential deposition of copper is not occurring. Reoxidation of the copper deposited on the gold must necessarily occur, but with significantly lower current values and masked by modifications of the microdisc surface due to the combined processes of reduction, deposition, oxidation, and redissolution, which seem to be the cause of the current oscillations observed in 10 and 100 mM.

3.2. Imaging of Copper Corrosion Using SECM Coupled with a Voltammetric Mode

In order to illustrate the ability of the Au microelectrode to locally determine Cu^{2+} ions arising from a corroding copper source, a metal surface consisting of a copper disc of 125 μm in diameter embedded in insulating resin was analysed. In order to precisely place the tip above the copper sample and establish a sensitive tip-substrate distance for mapping, an SECM operation was performed in the feedback mode using ferrocene-methanol as the redox mediator in a concentration of 0.5 mM. In order to minimise the corrosion of the copper substrate during the tip positioning step, this operation was performed in a more

dilute NaCl concentration (namely 0.5 M) without acidification. The positive feedback mode consists of determining the oxidation signal of an oxidisable complex through an outer sphere mechanism, such as ferrocene-methanol, which can also be regenerated from the oxidised form on conductive materials with an adequate electrical condition. On the contrary, if ferrocene-methanol, as a redox mediator, is oxidised at the tip of the SECM when it approaches the surface of the insulating resin adjacent to the metal, the diffusion-limited current of the mediator will be hindered. Numerical estimates make it possible to model the approach current profile and precisely determine the distance between the gold microdisc and the surface under study [47]. Figure 7 shows the approximation made on the resin by applying a potential of +0.4 V to the tip (thus, in the diffusion-limited regime of the mediator oxidation reaction). This fit was carried out by considering the distance and the normalised current that corresponds to the ratio between the current measured at each location to the limiting diffusion value measured in the bulk of the solution. A normalised distance L was also employed, that is obtained by dividing the actual Z value by the radius of the microdisc (i.e., 5 μm).
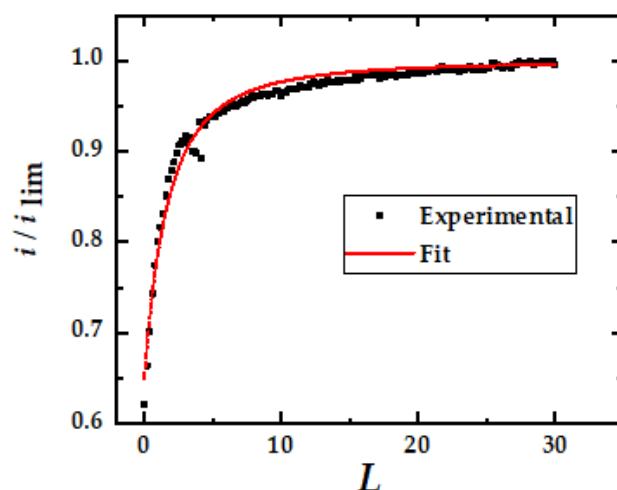

Figure 7. Z-approach curve recorded with the 10 μm diameter Au tip on the insulating resin surface surrounding a copper wire of 125 μm diameter immersed in a neutral 0.5 M NaCl + 0.5 mM ferrocene-methanol solution. The red line shows the fit according to the model described in reference [47].

The fit also provides geometric information relating to the diameter of the glass body of the tip that surrounds the gold disc of the microelectrode. In our case, the glass disc at the tip was 11 times larger than the gold microdisc. Additionally, it was determined that the height $L = 0$ at which the approach was stopped actually corresponded to a real distance of 1.65 times the radius of the microdisc (i.e., 8.25 μm). Next, while maintaining this distance between the tip and the sample, a two-dimensional scan was performed to locate the copper wire surrounded by the resin. To do this, we exploited the capacity of copper to regenerate the redox mediator and thus locally increase the current when the tip passes over it, which was observed in the map shown in Figure 8. Once the sample was located, the electrode was held over its position at the same distance of 8.25 μm and the solution was replaced with a 0.5 M NaCl solution at pH = 3 but without containing ferrocene-methanol. It must be noted that in this acidic electrolyte, copper corrosion is distributed over the complete exposed surface with a behaviour that is often described as homogeneous corrosion. That is, although copper dissolution will not happen in a heterogeneous manner in this case, the goal was rather to be able to obtain signals related to copper dissolution in real time with the SECM tip that could be associated with positions in the surface to achieve spatial resolution. Once the proof of concept is demonstrated, the methodology can be extended to the investigation of copper-based materials under conditions of localised corrosion, a work currently underway at our laboratory.
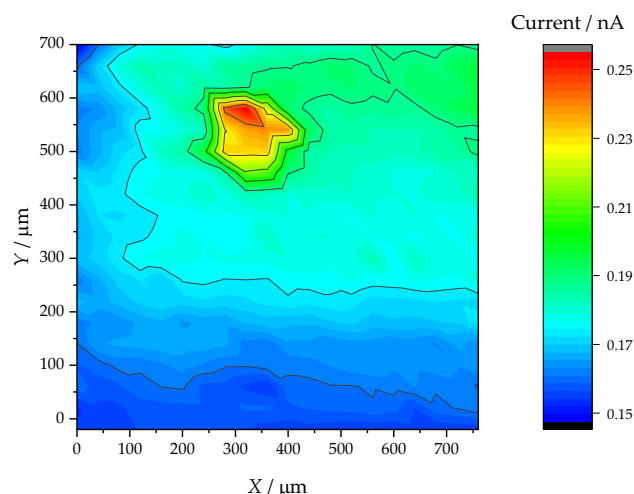
Figure 8. SECM map obtained in positive feedback mode on a circular copper surface of 125 μm in diameter immersed in 0.5 M NaCl + 0.5 mM ferrocene-methanol. Electrochemically active sites on the copper surface can regenerate the reduced state of ferrocene-methanol and higher local currents are measured at the tip compared with the values measured when the tip is located over the insulating resin, because the geometric blocking of the sample and the tip hinders the supply of ferrocene-methanol from the bulk solution.

Once the sample was connected as the second working electrode, voltammograms were recorded at the tip while a constant potential was applied to the copper sample. These measurements were conducted with the tip placed directly over the copper substrate. In this way, the amount of dissolved copper present near its surface could be quantified with the gold microelectrode as the first working electrode, because the anodic dissolution conditions of the sample were forced. No significant signal was obtained until the sample was polarised at –0.1 V. Figure 9A shows the current transferred by the substrate for each experiment, and Figure 9B shows the cyclic voltammogram obtained simultaneously at the tip.
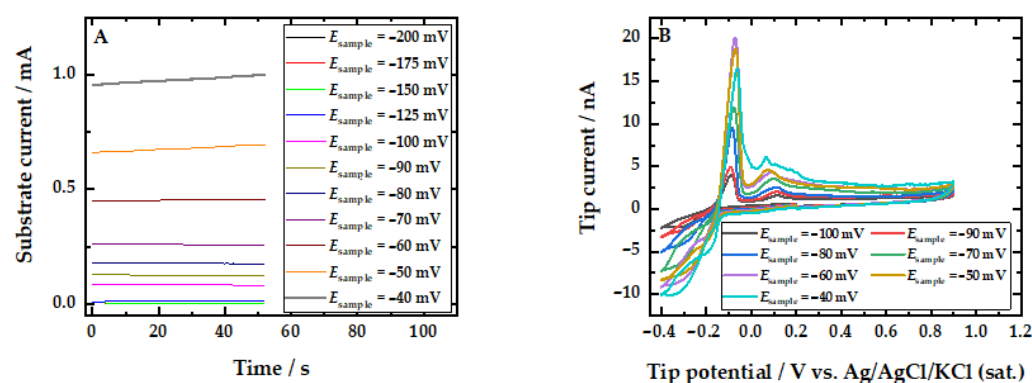

Figure 9. Amperometric responses: (**A**) current flowing through the copper substrate, and (**B**) cyclic voltammograms recorded simultaneously at the gold microelectrode placed above the copper. The copper surface was polarised at the values indicated in the legends. Test solution: 0.5 M NaCl (pH = 3). Tip-sample distance: 8 μm.

Voltammograms recorded at the tip showed cathodic diffusion current signals and reoxidation peaks that allow for quantification of the amount of copper present in the electrolyte at approximately 8 μm from the surface. Concerning the limit currents, the possibility of transforming them directly into current values using Equation (2) [9] makes it possible to compare the current values transferred by the sample (by means of current density) at the end of each experiment, with the apparent concentration determined using the microelectrode. As shown in Figure 10, concentration values between 0.5 and 4 mM

are obtained, consistent with the emerge of an anodic stripping signal not leading to high activity and being able to initiate passivation phenomena.
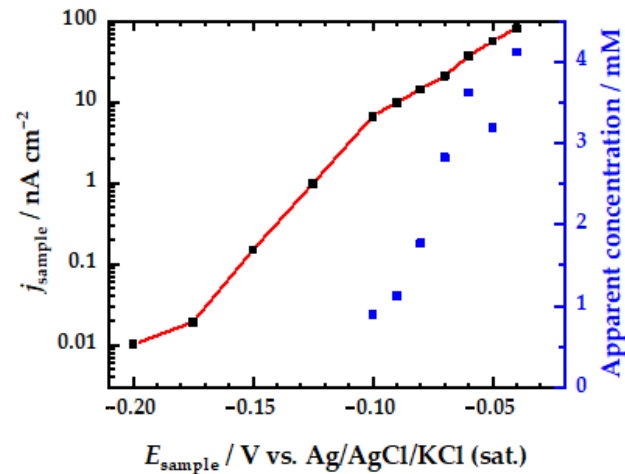
$$i_{\lim} = 4nFDr_0c \tag{2}$$

Figure 10. Current density measured in the sample (left axis, black dots) and apparent concentration of Cu^{2+} in the electrolyte (right axis, blue dots) detected by the microelectrode as a function of the potential applied to the sample. Test solution: 0.5 M NaCl (pH = 3).

From the inspection of Figure 10, it is shown that the release of copper ions is not appreciable until a potential equal or more positive than −0.1 V was reached. Next, the values obtained suggest comparing the reoxidation results with those obtained with the same test solution with $CuCl_2$ concentrations between 1 and 10 mM. Figure 11 shows the charges transferred during the reoxidation processes on the microelectrode, which again shows two reoxidation peaks due to the transformation of Cu into Cu^+ and then into Cu^{2+}. However, due to the use of a different reference electrode and experimental errors, the range of potentials used during cyclic voltammetry is not the same as that in the experiments carried out in the solution in the presence of salts of copper. This poses difficulties in the interpretation and extrapolation of the results. To resolve this problem, we corrected the charge transferred during the reoxidation by dividing it by the interval of the potential window, given in mV, in which the progress of the electroreduction of copper is observed. That is, the transferred charge values were divided by the potential window which begins at the start of the copper reduction wave during the cathode scan and which ends when the oxidation peak begins, providing the results in Figure 11B.
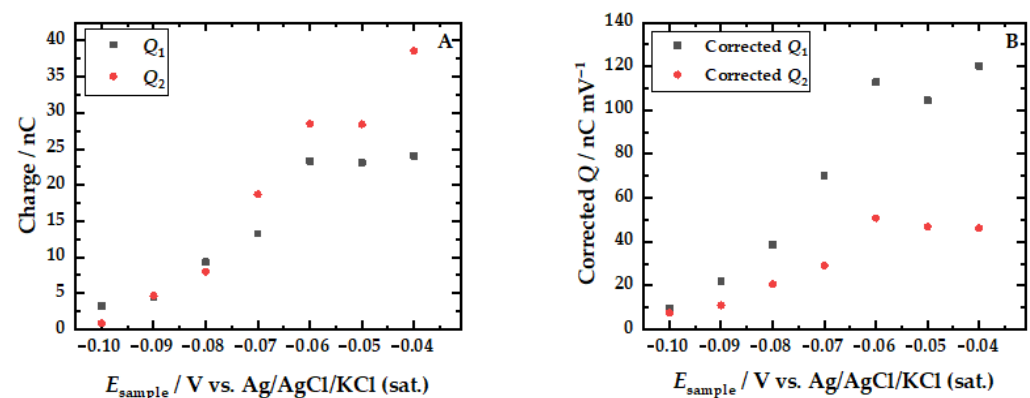

Figure 11. Potential dependence of the charge transferred during cyclic voltammograms measured with the gold microelectrode near the copper surface. (**A**) Total values of transferred charges. (**B**) Values corrected by dividing the transferred charge by the potential window in which copper reduction had previously occurred.

If we look at the transferred charge values without considering this correction, the reoxidation peaks give values between 3.2 at 24 nC for peak 1 and 0.84 at 39 nC for the second peak (Figure 11A). According to Figure 10, the concentration detected by the cathodic diffusion current was in the range of 0.9 to 4.2 nM. Tables 1 and 2 summarise the numerical values of the transferred charges quantified for these experiments and those carried out with the Au microelectrode in solutions containing $CuCl_2$ in concentrations of 1 and 10 mM (cf. Figure 3).

Table 1. Electron transfer near the surface of the microelectrode according to Figure 11.

Concentration/mM	Q_1/nC	Q_2/nC	Corrected Q_1/nC V^{-1}	Corrected Q_2/nC V^{-1}
0.90	3.25	0.84	9.66	7.66
1.12	4.55	4.65	22.1	10.9
1.77	9.32	8.03	38.5	20.7
2.83	13.3	18.7	70.3	29.2
3.62	23.3	28.5	113	50.8
3.19	23.1	28.4	104	46.9
4.12	24.1	38.6	120	46.2

Table 2. Electron transfer at the microelectrode in the bulk of the solution according to Figure 3.

Concentration/mM	Q_1/nC	Q_2/nC	Corrected Q_1/nC V^{-1}	Corrected Q_2/nC V^{-1}
1	13.9	2.4	19.9	3.42
10	219	124	260	148

Although the correlation is not perfect, even without applying the corrections, the trends in Table 1 are an order of magnitude lower than the 219 + 124 nC transferred for 10 mM (cf. Table 2). If corrections are applied, the value recorded for the first reoxidation peak is very similar to the experiment carried out with the microelectrode near the surface at a concentration equivalent to 1.12 mM (22.1 nC mV^{-1} in Table 1) that was carried out in a 1 mM $CuCl_2$ solution (19.9 nC mV^{-1} in Table 2). Similarly, the signal recorded for the near-surface microelectrode detecting an apparent concentration of 4.12 mM (120 nC mV^{-1} in Table 1) represents just over 40% of the signal corrected for 10 mM in Table 2 (260 nC mV^{-1}). The first peak being the most determining in the presence of chloride ions, these similarities reveal acceptable results, taking into account the differences which exist compared with an experiment carried out within the solution and an experiment carried out near a metallic substrate: (1) the local pH may vary during the release of Cu^{2+} ions from the metal (substrate); and (2) the diffusion conditions from the tip and from the substrate are not equivalent to those in the core of the solution when it confines a very small volume.

Finally, the imaging of a copper corrosion experiment was performed using a larger coupon of non-circular shape, as shown in Figure 12A. Now, Figure 12B shows a 3D SECM map obtained in feedback mode of a section of the unbiased copper sample, indicated by the square drawn in Figure 12A. This 3D map was recorded over a 500 × 500 μm^2 area that partially covers the metal and the surrounding resin to observe differences in electrochemical behaviour when the sample was immersed in a solution of composition 0.1 M $NaClO_4$ + 0.5 mM ferrocene-methanol (in order to minimise the corrosion rates in a chloride-free and non-acidic environment). Figure 12B shows a large variation in the currents measured at the tip depending on whether it moved above the organic resin or the metal. Since the metal has the capacity to regenerate the redox mediator on its surface by providing electrons from its valence band even if polarisation is not applied, greater redox mediator concentrations are found by the tip placed over the metal, whereas the resin is a dielectric insulator incapable of supporting a redox reaction. Therefore, the tip

monitored faradic current values close to zero when it was placed above the resin in the region $0 \leq Y \leq 150$ µm.
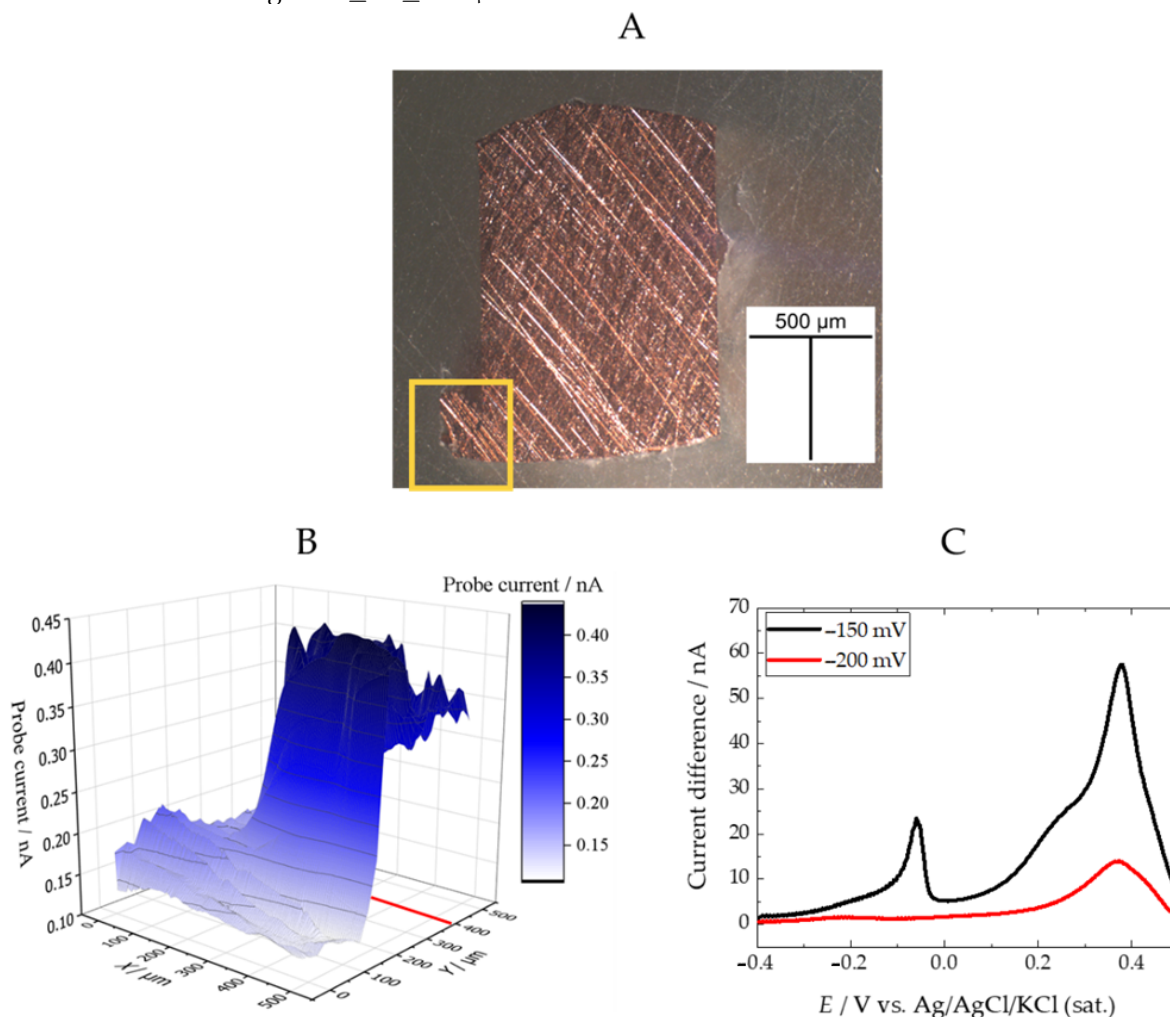

Figure 12. (**A**) Optical micrograph of the copper sample. The square indicates the approximate region imaged using SECM (500 × 500 µm^2). (**B**) Three-dimensional SECM map in feedback mode (tip potential: +0.5 V) of the copper sample immersed in 0.1 M NaClO$_4$ + 0.5 mM ferrocene-methanol solution. (**C**) Square-wave voltammogram recorded with the gold tip moving over the copper (line along Y = 400 µm position, that is highlighted as a red line in (**B**)). The copper substrate was (**B**) unbiased and (**C**) polarised as indicated in the legends. Tip-substrate distance: 10 µm; tip diameter: 10 µm; rastering speed: 30 µm s^{-1}.

After electrolyte removal with the 3.5 wt.% NaCl solution acidified to pH 3.5, a series of square-wave voltammetric runs were performed at the Au tip to collect the copper released by the corrosion process, followed by its corresponding stripping to recover the originally copper-free condition of the Au disk. These measurements were performed simultaneously with the tip travelling the 500 × 500 µm^2 area. This procedure helps to discriminate different corrosion rates in the investigated surface arising from either local heterogeneities or differences in anodic activation of the copper substrate. The latter is the case for the square-wave voltammograms shown in Figure 12C that were recorded along the scan line for Y = 400 µm in Figure 12B (that is, indicated by the red line plotted in the graph). They were for two different polarisations applied to the copper surface. When the polarisation value of the copper substrate was −200 mV, copper dissolution due to corrosion was still sufficiently low as to find only one voltammetric peak at around +0.35 V. That is, it closely matched the electrochemical behaviour observed in Figure 5A for the Au microelectrode in solutions with CuCl$_2$ concentrations not bigger than 0.1 mM.

A very distinctive situation is observed for the corresponding square-wave voltammetric curve recorded when a more anodic polarisation was applied to the substrate, namely −150 mV. Voltammetric signals are observed now in two distinctive potential ranges, similarly to the behaviour depicted in Figure 5B. Therefore, a relevant acceleration of the copper corrosion reaction leading to enhanced copper dissolution occurred by shifting the anodic polarisation by 50 mV in the positive direction of potential, high enough for the complete surface of the Au tip to be coated by Cu, leading to multilayer copper deposition, which is stripped at more negative potentials than for the copper directly deposited on Au. Although the shapes of the voltammetric curves In Figure 12C are notoriously different in terms of shape and number of peaks, they correlate well with the investigations in Section 3.2 corresponding to the electrochemical behaviour of a Au microelectrode in acidic solutions of varying Cu^{2+} ion concentrations. Thus, polarisation of the copper sample at −200 mV leads to a voltammetric curve very similar to those reproduced in Figure 5A for $CuCl_2$ concentrations below 0.1 mM, while a more anodic polarisation at −150 mV shows two peaks as already found in Figure 5B for higher Cu^{2+} concentrations, as would be expected for a higher corrosion rate of the metal. Furthermore, the changes in the shape of the voltammograms related to the different concentration distributions of the soluble copper corrosion products and the potential ranges of the voltammetric characteristics could only be properly attributed and quantified when the electrochemical characterisation of the Au electrode used for SECM imaging was performed with a microelectrode of similar shape and dimensions to the SECM tip, and not with electrochemical data obtained using larger (conventional) electrodes. This fact can be readily concluded by observing the different shapes and voltammetric characteristics in the cyclic voltammograms in Figures 2A and 3B and in the square-wave voltammograms in Figures 2B and 5B, which differed only in the size of the Au electrode used.

Although the above discussed results are of a very preliminary nature in regard to the precise quantification of the corrosion of copper in an acidic environment containing chloride ions, they prove the power of the technique to detect in situ the positioning of localised microcells developed on the material both in a freely corroding substrate and when subjected to controlled polarisation conditions, and the extent of their anodic activation. Experiments are currently underway in our laboratory in order to exploit this effect in real corrosion conditions by using Au microelectrodes as tips, and by coupling voltammetric measurements with the amperometric SECM operation.

4. Conclusions

The capabilities and limitations of potentiodynamic SECM methods to locally reveal surface features due to chemical information of interest, distinguishing active sites or areas in corrosion processes, have been investigated in order to develop a methodology to image the local release of copper as determined over the metal surface undergoing degradation. Voltammetric methods have been tested to identify the signals of interest for corrosion detection and quantification.

It has been observed that even In the case of classical electrochemical techniques, such as voltammetric methods, the microelectrodes provide a better response than the macroelectrodes, on the quantitative level, on the chemical species studied, in this case the Cu^{2+} ions released during corrosion.

It is possible to quantify the concentration of Cu^{2+} ions using a gold microelectrode in the presence of Cl^{-} anions using cyclic voltammetry. In this environment, the first reoxidation peak is the most relevant because it releases most of the copper deposited in the form of the copper(I) species. However, the limiting current reached by the microelectrode during the electroreduction of Cu^{2+} is a more reliable parameter for quantification only at the end of the reduction wave before the electrode surface area increases due to deposition.

The use of SECM made it possible to obtain electrochemical surface information at the local scale, allowing us to differentiate current signals between zones separated by a few micrometres. However, it has some limitations that could be counteracted by the use

of complementary techniques that would allow one to obtain more information about the material under study, such as the dynamic combinations of voltammetry with the SECM employed in this work. The information derived from the reoxidation peaks represents a semi-quantitative result sensitive to the experimental conditions of the potential window applied to the copper surface to modify the corrosion rates.

Under conditions close to a marine environment, the release of Cu^{2+} ions can be unequivocally detected and quantified from potentials above –0.1 V.

Author Contributions: Conceptualisation, J.I.; investigation, B.H.-C., A.M.-G. and J.I.; methodology, J.I. and R.M.S.; writing—original draft preparation, B.H.-C., J.I. and R.M.S.; writing—review and editing, J.I. and R.M.S.; visualisation, J.I.; funding acquisition, R.M.S. All authors have read and agreed to the published version of the manuscript.

Data Availability Statement: The raw/processed data required to reproduce these findings cannot be shared at this time as the data also form part of an ongoing study. They will be available on request.

Conflicts of Interest: The authors declare no conflict of interest.

References

1. Pistorius, P.C.; Burstein, G.T. Metastable pitting corrosion of stainless steel and the transition to stability. *Philos. Trans. R. Soc. London. Ser. A Phys. Eng. Sci.* **1992**, *341*, 531–559.
2. Montemor, M.F. Corrosion issues in joining lightweight materials: A review of the latest achievements. *Phys. Sci. Rev.* **2016**, *1*, 20150011. [CrossRef]
3. Liu, W.; Yang, H.; Li, X.; Zhang, Z.; Lin, Y.; Deng, K. Effect of chloride and iodide on the corrosion behavior of 13Cr stainless steel. *Metals* **2022**, *12*, 1833. [CrossRef]
4. Zhou, P.; Deng, L.; Guo, P.; Rao, W.; Wang, X.; Zhang, M. Influence of microstructure heterogeneity on the corrosion resistance and microhardness of 5052 Al-Mg alloy. *J. Mater.* **2020**, *72*, 4305–4314.
5. Li, X.-R.; Meng, X.-Z.; Zhang, Q.-H.; Wu, L.-K.; Sun, Q.-Q.; Deng, H.-Q.; Sun, S.-J.; Cao, F.-H. Insight into oxygen reduction activity and pathway on pure titanium using scanning electrochemical microscopy and theoretical calculations. *J. Colloid Interface Sci.* **2023**, *643*, 551–562. [CrossRef] [PubMed]
6. Raj Xavier, J.; Ramesh, B. A study on the effect of multifunctional tantalum carbide nanofillers incorporated graphene oxide structure in the epoxy resin for the applications in the shipbuilding industry. *Mater. Sci. Eng. B* **2023**, *289*, 116234. [CrossRef]
7. Payne, N.A.; Stephens, L.I.; Mauzeroll, J. The application of scanning electrochemical microscopy to corrosion research. *Corrosion* **2017**, *73*, 759–780. [CrossRef] [PubMed]
8. Traxler, I.; Singewald, T.D.; Schimo-Aichhorn, G.; Hild, S.; Valtiner, M. Scanning electrochemical microscopy methods (SECM) and ion-selective microelectrodes for corrosion studies. *Corros. Rev.* **2022**, *40*, 515–542. [CrossRef]
9. Kwak, J.; Bard, A.J. Scanning electrochemical microscopy. Theory of the feedback mode. *Anal. Chem.* **1989**, *61*, 1221–1227. [CrossRef]
10. Bard, A.J.; Denuault, G.; Lee, C.; Mandler, D.; Wipf, D.O. Scanning electrochemical microscopy—A new technique for the characterization and modification of surfaces. *Acc. Chem. Res.* **1990**, *23*, 357–363. [CrossRef]
11. Bard, A.J. Introduction and principles. In *Scanning Electrochemical Microscroscopy*, 3rd ed.; Bard, A.J., Mirkin, M.V., Eds.; CRC Press: Boca Raton, FL, USA, 2022; pp. 1–10.
12. Mirkin, M.V.; Nogala, W.; Velmurugan, J.; Wang, Y. Scanning electrochemical microscopy in the 21st century. Update 1: Five years after. *Phys. Chem. Chem. Phys.* **2011**, *13*, 21196–21212. [CrossRef] [PubMed]
13. Noël, J.-M.; Kanoufi, F. Probing the reactive intermediate species generated during electrocatalysis by scanning electrochemical microscopy. *Curr. Opin. Electrochem.* **2022**, *35*, 101071. [CrossRef]
14. Zhang, J.; Zhu, T.; Lang, J.; Fu, W.; Li, F. Scanning electrochemical microscopy of living cells. *Curr. Opin. Electrochem.* **2020**, *22*, 178–185. [CrossRef]
15. Hill, C.M.; Pan, S. SECM techniques for locally interrogating the photocatalytic activity of semiconducting materials for solar-driven transformations. In *Scanning Electrochemical Microscroscopy*, 3rd ed.; Bard, A.J., Mirkin, M.V., Eds.; CRC Press: Boca Raton, FL, USA, 2022; pp. 361–378.

16. Kranz, C.; Demaille, C. Hybrid scanning electrochemical techniques: Methods and applications. In *Scanning Electrochemical Microscroscopy*, 3rd ed.; Bard, A.J., Mirkin, M.V., Eds.; CRC Press: Boca Raton, FL, USA, 2022; pp. 513–580.
17. Heurtault, S.; Robin, R.; Rouillard, F.; Vivier, V. On the propagation of open and covered pit in 316L stainless steel. *Electrochim. Acta* **2016**, *203*, 316–325. [CrossRef]
18. Hampel, M.; Schenderlein, M.; Schary, C.; Dimper, M.; Ozcan, O. Efficient detection of localized corrosion processes on stainless steel by means of scanning electrochemical microscopy (SECM) using a multi-electrode approach. *Electrochem. Commun.* **2019**, *101*, 52–55. [CrossRef]
19. Blanc, C.; Pébère, N.; Tribollet, B.; Vivier, V. Galvanic coupling between copper and aluminium in a thin-layer cell. *Corros. Sci.* **2010**, *52*, 991–995. [CrossRef]
20. Yan, Z.-Z.; Zhang, Q.-H.; Cai, H.-R.; Li, X.-R.; Wu, L.-K.; Luo, Z.-Z.; Cao, F.-H. Study on the galvanic corrosion of titanium and stainless steel couple with the synergistic effect of proton and fluoride ion. *Corros. Sci.* **2022**, *206*, 110541. [CrossRef]
21. Pal, A.; Krishna, N.G.; Shantar, A.R.; Philip, J. High contrast corrosion mapping of dissimilar metal weld joints using alternating current scanning electrochemical microscopy: A case study with Zr-4–Ti–304L SS weld. *Corros. Sci.* **2023**, *221*, 111345. [CrossRef]
22. Martinez-Lombardia, E.; Gonzalez-Garcia, Y.; Lapeire, L.; De Graeve, I.; Verbeken, K.; Kestens, L.; Mol, J.M.C.; Terryn, H. Scanning electrochemical microscopy to study the effect of crystallographic orientation on the electrochemical activity of pure copper. *Electrochim. Acta* **2014**, *116*, 89–96. [CrossRef]
23. Lin, E.; Li, X.; Kure-Chu, S.-Z.; Li, X.; Xiao, X. Effect of electrical parameters on the microstructure and corrosion resistance of anodized film of Mg-1Zn-1Gd alloy based on orthogonal experiment method. *J. Mater. Eng. Perform.* **2023**, *in press*. [CrossRef]
24. Nickchi, T.; Rostron, P.; Barsoum, I.; Alfantazi, A. Measurement of local galvanic surface corrosion using scanning electrochemical microscopy on ductile cast iron. *J. Mater. Sci.* **2019**, *54*, 9213–9221. [CrossRef]
25. Sidane, D.; Devos, O.; Puiggali, M.; Touzet, M.; Tribollet, B.; Vivier, V. Electrochemical characterization of a mechanically stressed passive layer. *Electrochem. Commun.* **2011**, *13*, 1361–1364. [CrossRef]
26. Grandy, L.; Mauzeroll, J. Localising the electrochemistry of corrosion fatigue. *Curr. Opin. Colloid Interface* **2022**, *61*, 101628. [CrossRef]
27. Pust, S.E.; Scharnweber, D.; Kirchner, C.N.; Wittstock, G. Electron transfer kinetics at oxide films on metallic biomaterials. *Adv. Mater.* **2007**, *19*, 878–882. [CrossRef]
28. Meiszterics, Z.; Kiss, A.; Nagy, L.; Zsebe, T.; Vasvári, G.F.; Csonka, D.C.; Nagy, G. Investigation of the regeneration of the passive surface oxide layer of TiAl6V4 alloy printed by WAAM technology using different electrochemical test methods. *Electroanalysis* **2023**, *35*, e202200506. [CrossRef]
29. Xia, D.H.; Wang, J.; Wu, Z.; Qin, Z.; Xu, L.; Hu, W.; Behnamian, Y.; Luo, J.L. Sensing corrosion within an artificial defect in organic coating using SECM. *Sens. Actuat. B Chem.* **2019**, *280*, 235–242. [CrossRef]
30. Santana, J.J.; Izquierdo, J.; Souto, R.M. Uses of scanning electrochemical microscopy (SECM) for the characterization with spatial and chemical resolution of thin surface layers and coating systems applied on metals: A review. *Coatings* **2022**, *12*, 637. [CrossRef]
31. Liang, J.; Liu, S.; Peng, Z.; Li, R.; Wang, B. Galvanic corrosion behavior of AZ31 Mg alloy coupled with mild steel: Effect of coatings. *J. Mater. Res. Technol.* **2023**, *24*, 7745–7755. [CrossRef]
32. Zhang, Y.; Liu, X.; Jamal, S.S.; Hinton, B.R.W.; Moulton, S.E.; Wallace, G.G.; Forsyth, M. The effect of treatment time on the ionic liquid surface film formation: Promising surface coating for Mg alloy AZ31. *Surf. Coat. Technol.* **2016**, *296*, 192–202. [CrossRef]
33. Xavier, J.R. Superior surface protection, mechanical and hydrophobic properties of silanized tungsten carbide nanoparticles encapsulated epoxy nanocomposite coated steel structures in marine environment. *Silicon* **2022**, *14*, 11147–11161. [CrossRef]
34. Niaz, A.; Al Fuhaid, A.F.; Faraz, M.I. Understanding corrosion degradation processes of a multi-component CoNiCrAlY-coating system. *Coatings* **2022**, *12*, 1396. [CrossRef]
35. Al-Jeda, M.; Mena-Morcillo, E.; Chen, A. Micro-sized pH sensors based on scanning electrochemical probe microscopy. *Micromachines* **2022**, *13*, 2143. [CrossRef] [PubMed]
36. Zhao, G.; Liang, R.; Wang, F.; Ding, J.; Qin, W. An all-solid-state potentiometric microelectrode for detection of copper in coastal sediment pore water. *Sens. Actuat. B-Chem.* **2019**, *279*, 369–373. [CrossRef]
37. Varvara, S.; Caniglia, G.; Izquierdo, J.; Bostan, R.; Găină, L.; Bobis, O.; Souto, R.M. Multiscale electrochemical analysis of the corrosion control of bronze in simulated acid rain by horse-chestnut (*Aesculus hippocastanum* L.) extract as green inhibitor. *Corros. Sci.* **2020**, *165*, 108381. [CrossRef]
38. Izquierdo, J.; Fernández-Pérez, B.M.; Eifert, A.; Souto, R.M.; Kranz, C. Simultaneous atomic force-scanning electrochemical microscopy (AFM-SECM) imaging of copper dissolution. *Electrochim. Acta* **2016**, *201*, 320–332. [CrossRef]
39. Izquierdo, J.; Eifert, A.; Kranz, C.; Souto, R.M. In situ investigation of copper corrosion in acidic chloride solution using atomic force-scanning electrochemical microscopy. *Electrochim. Acta* **2017**, *247*, 588–599. [CrossRef]
40. Schrock, D.S.; Baur, J.E. Chemical imaging with combined fast-scan cyclic voltammetry-scanning electrochemical microscopy. *Anal. Chem.* **2007**, *79*, 7053–7061. [CrossRef]
41. Barton, Z.J.; Rodríguez-López, J. Cyclic voltammetry probe approach curves with alkali amalgams at mercury sphere-cap scanning electrochemical microscopy probes. *Anal. Chem.* **2017**, *89*, 2708–2715. [CrossRef]
42. Bard, A.J.; Faulkner, L.R.; White, H.S. *Electrochemical Methods: Fundamentals and Applications*, 3rd ed.; John Wiley & Sons: New York, NY, USA, 2022.

43.   Harris, K.R.; Woolf, L.A. Pressure and temperature dependence of the self diffusion coefficient of water and oxygen-18 water. *J. Chem. Soc. Faraday Trans.* **1980**, *76*, 377–385. [CrossRef]
44.   Yu, Y.; Gao, Y.; Hu, K.; Blanchard, P.Y.; Noël, J.M.; Nareshkumar, T.; Phani, K.L.; Friedman, G.; Gogotsi, Y.; Mirkin, M.V. Electrochemistry and electrocatalysis at single gold nanoparticles attached to carbon nanoelectrodes. *ChemElectroChem* **2015**, *2*, 58–63. [CrossRef]
45.   Papaderakis, A.; Anastopoulos, A.G.; Sotiropoulos, S. Electrochemical studies of processes occurring at the polycrystalline Cu electrode/methanol interface. *J. Electroanal. Chem.* **2016**, *783*, 217–225. [CrossRef]
46.   Krznarić, D.; Goričnik, T. Reactions of copper on the Au(111) surface in the underpotential deposition region from chloride solutions. *Langmuir* **2001**, *17*, 4347–4351. [CrossRef]
47.   Cornut, R.; Lefrou, C. New analytical approximation of feedback approach curves with a microdisk SECM tip and irreversible kinetic reaction at the substrate. *J. Electroanal. Chem.* **2008**, *621*, 178–184. [CrossRef]